OPEN ACCESS Freely available online

PLoS GENETICS

Viral Genome Segmentation Can Result from a Trade-Off between Genetic Content and Particle Stability

Samuel Ojosnegros[1¤a], Juan García-Arriaza[1,2], Cristina Escarmís[1], Susanna C. Manrubia[3], Celia Perales[1], Armando Arias[1¤b], Mauricio García Mateu[1], Esteban Domingo[1,4]*

1 Centro de Biología Molecular "Severo Ochoa," CSIC-UAM, Madrid, Spain, **2** Centro Nacional de Biotecnología, CSIC, Madrid, Spain, **3** Laboratorio de Evolución Molecular, Centro de Astrobiología (CSIC/INTA), Instituto Nacional de Técnica Aeroespacial, Madrid, Spain, **4** Centro de Investigación Biomédica en Red de Enfermedades Hepáticas y Digestivas (CIBERehd), Barcelona, Spain

Abstract

The evolutionary benefit of viral genome segmentation is a classical, yet unsolved question in evolutionary biology and RNA genetics. Theoretical studies anticipated that replication of shorter RNA segments could provide a replicative advantage over standard size genomes. However, this question has remained elusive to experimentalists because of the lack of a proper viral model system. Here we present a study with a stable segmented bipartite RNA virus and its ancestor non-segmented counterpart, in an identical genomic nucleotide sequence context. Results of RNA replication, protein expression, competition experiments, and inactivation of infectious particles point to a non-replicative trait, the particle stability, as the main driver of fitness gain of segmented genomes. Accordingly, measurements of the volume occupation of the genome inside viral capsids indicate that packaging shorter genomes involves a relaxation of the packaging density that is energetically favourable. The empirical observations are used to design a computational model that predicts the existence of a critical multiplicity of infection for domination of segmented over standard types. Our experiments suggest that viral segmented genomes may have arisen as a molecular solution for the trade-off between genome length and particle stability. Genome segmentation allows maximizing the genetic content without the detrimental effect in stability derived from incresing genome length.

Citation: Ojosnegros S, García-Arriaza J, Escarmís C, Manrubia SC, Perales C, et al. (2011) Viral Genome Segmentation Can Result from a Trade-Off between Genetic Content and Particle Stability. PLoS Genet 7(3): e1001344. doi:10.1371/journal.pgen.1001344

Editor: Harmit S. Malik, Fred Hutchinson Cancer Research Center, United States of America

Received September 3, 2010; **Accepted** February 16, 2011; **Published** March 17, 2011

Funding: Work at Centro de Biologia Molecular Severo Ochoa was supported by grants BFU2006-00863 from MEC, BFU2008-02816/BMC from MCI, 36558/06 from FIPSE, and Fundacion R. Areces. CIBERehd is funded by Instituto de Salud Carlos III. SO was supported by a predoctoral fellowship from the MEC. The funders had no role in study design, data collection and analysis, decision to publish, or preparation of the manuscript.

Competing Interests: The authors have declared that no competing interests exist.

* E-mail: edomingo@cbm.uam.es

¤a Current address: California Institute of Technology, Division of Biology, Pasadena, California, United States of America
¤b Current address: Department of Virology, Imperial College London, London, United Kingdom

Introduction

A biological clone of foot-and-mouth disease virus (FMDV), termed C-S8c1, evolved in BHK-21 cell culture infections at high multiplicity of infection (MOI), towards a population dominated by defective genomic forms that were infectious by complementation in the absence of standard size (ST) genomes [1] (Figure 1 and Figure S1). By passage 260, the population (C-S8p260) was composed mainly of two classes of genomes that included internal in-frame deletions, Δ417 plus Δ999 and the minority genome Δ1017 (with deletions of 417, 999 and 1017 nucleotides, respectively, at the capsid-coding region). ST genomes were not detected in C-S8p260, and it was estimated that their frequency in C-S8p260 was lower than 10^{-4}-fold the frequency of genomes with deletions. The segmented genome version was stable at least up to passage 460 at high MOI. However, when population C-S8p260 was subjected to low-MOI infections, that impeded coinfection of cells by the complementing genome classes, a ST genome termed C-S8p260p3d was selected as a result of recombination between Δ417 and Δ999 RNAs (Figure S1) [2]. The dominance of a population of complementing defective genomes that did not require ST genomes for replication was regarded as the first step of an evolutionary transition towards viral genome segmentation, an event likely to have occurred at some point of the evolutionary history of RNA viruses [1,3–6]. A critical question in the displacement of a ST genome by defective, complementing genomes, is the molecular basis that underlies the superiority of the segmented forms over the ST genome. As C-S8p260 and C-S8p260p3d share a common genetic background (similar set of point mutations relative to the parental C-S8c1), this dual viral system constitutes a suitable model to address this fundamental question [2].

Here we provide evidence that the segmented C-S8p260 is endowed with a non replicative advantage over its unsegmented counterpart C-S8p260p3d that does not reside in the rate of either RNA genome replication or of virus-specific protein synthesis. Unexpectedly, an increased virion stability conferred a higher specific infectivity and longer lifespan on the segmented virus.

Results

Fitness advantage of the segmented FMDV genome

The relative fitness advantage that led to dominance of the segmented population C-S8p260 over its ST ancestor was

Author Summary

Genome segmentation, the splitting of a linear genome into two or more segments, is a major evolutionary transition from independent towards complementing transmission of genetic information. Many viruses with RNA as genetic material have segmented genomes, but the molecular forces behind genome segmentation are unknown. We have used foot-and-mouth disease virus to address this question, because this non-segmented RNA virus became segmented into two RNAs when it was extensively propagated in cell culture. This made possible a comparison of the segmented form (with two shorter RNAs enclosed into separate viral particles) with its exactly matching non-segmented counterpart. The results show that the advantage of the segmented form lies in the higher stability of the particles that enclose the shorter RNA, and not in any difference in the rate of RNA synthesis or expression of the genetic material. Genome segmentation may have arisen as a molecular mechanism to overcome the trade-off between genomic content and particle stability. It allows optimizing the amount of genetic information while relaxing packaging density.

determined using virus-competition assays between C-S8p260 and C-S8p260p3d, or each in competition with $C^{9}{}_{22}$L150, another C-S8c1-derived clone of lower fitness (see Materials and Methods). Additionally, C-S8p260 was competed against the ST population derived from passage 460 (C-S8p460p5d) [2]. The results (Table 1 and Figure 2) indicate that population C-S8p260 displayed a two-fold higher fitness (or relative selection coefficient, see Materials and Methods) than C-S8p260p3d and C-S8p460p5d. Both, C-S8p260 and C-S8p260p3d won their respective competitions against $C^{9}{}_{22}$L150, but C-S8p260 displayed a 1.7-fold higher fitness than C-S8p260p3d. The outcome of these competitions strongly suggests that the segmented genetic system confers approximately a two-fold additional fitness advantage (relative to the corresponding unsegmented genome version), in agreement with its reaching dominance in the C-S8c1 lineage.

Kinetics of RNA synthesis

To identify the step of the virus life cycle that was associated with the fitness advantage of C-S8p260 over C-S8p260p3d, the intracellular and extracellular concentrations of viral RNA, in the course of infections with both viruses, were determined. BHK-21 cells were infected at a MOI of 20 PFU/cell, in order to maintain the coinfection of cells by the two components of C-S8p260, and to restrict the measurements to a single round of cell infections. In independent infections carried out in parallel (Figure 3A), C-S8p260 and C-S8p260p3d did not differ significantly in their exponential increase of intracellular viral RNA. Their respective growth rate constants (see Materials and Methods) were $r_{C\text{-}S8p260} = 0.065 \pm 0.007$ RNA molecules/cell·min and $r_{C\text{-}S8p260p3d} = 0.054 \pm 0.006$ molecules/cell·min (ANOVA, $F_{1,12} = 1.29$, $p = 0.278$). To test whether the selective advantage of C-S8p260 was manifested only upon coinfection with the unsegmented form, the specific RNA concentrations of C-S8p260 and C-S8p260p3d were measured in cells coinfected at high-MOI at the stages of cell entry (Figure 3B), intracellular replication (Figure 3C), and virus release to the extracellular medium (Figure 3D). Both types of RNA were rapidly

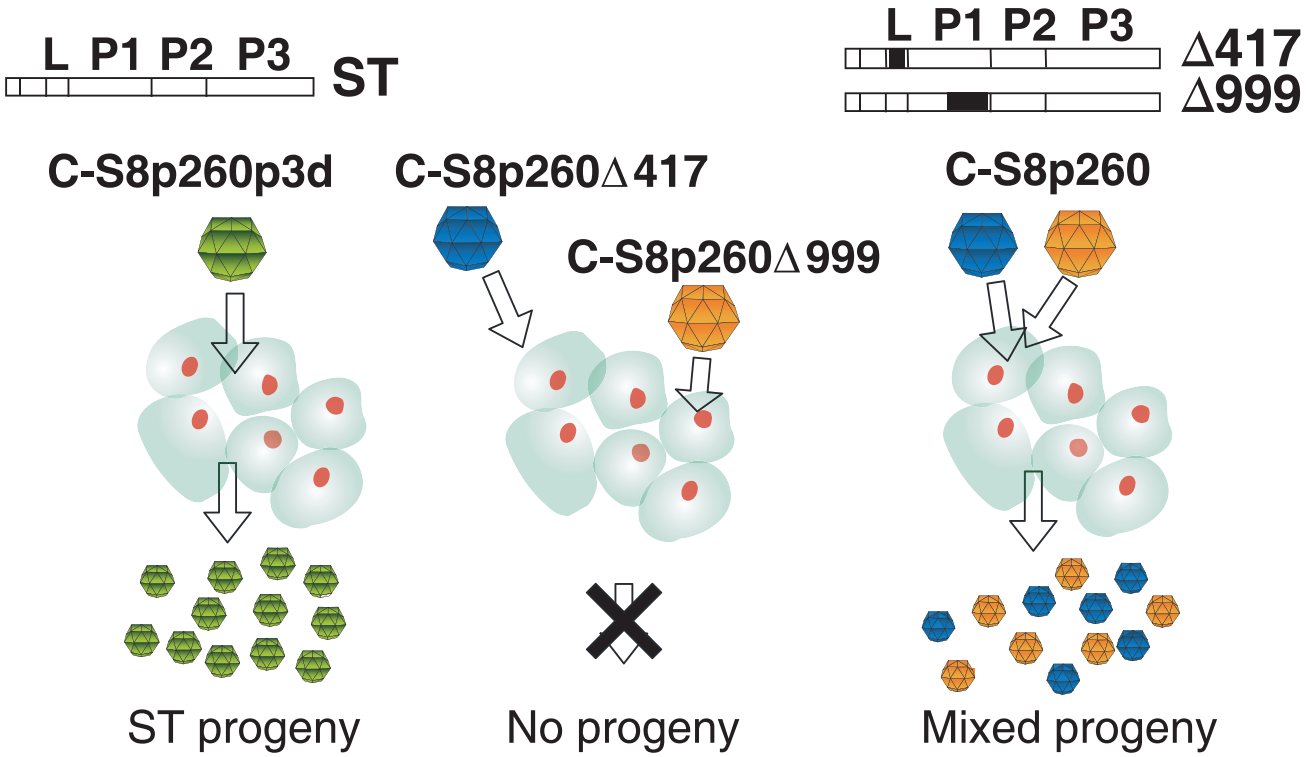

Figure 1. Schematic representation of the segmented and ST virus. The illustration shows the requirement of double infection for complementation and progeny production by the segmented FMDV population C-S8p260, but not by its ST derivative C-S8p260p3d [1,2]. A scheme of the FMDV genome with indication of the four main coding regions (L, P1, P2, P3) and the position of the internal deletions (Δ, black boxes) is drawn for each genotype.
doi:10.1371/journal.pgen.1001344.g001

Table 1. Relative fitness values obtained from virus competition experiments.

	C-S8p260p3d	C-S8p460p5d	C^{9}_{22}L150	C-S8p460
C-S8p260	2.5±0.005* 2.5±0.15[a]**	2.2±0.12**	3.5±0.1*	[C-S8p460[b]]p.d.
C-S8p260p3d	–	n.d.	2.0±0.15**	n.d.

Viruses in the first column were competed against the viruses indicated in the first row. The values correspond to the viruses listed in the first column and represent an estimation of the selection coefficient for one strain relative to the other (see Materials and Methods).

[a]This competition was carried out using the ratio 1:1 of C-S8p260 over C-S8p260p3d.

[b]p.d., previous determination. The selective advantage of C-S8p460 over C-S8p260 was previously documented by nucleotide sequence of the population that resulted after a competition between the two viruses [2].

n.d., not determined.

Null hypothesis rejection,

*T-Student, $p<0.01$,

**T-Student, $p<0.05$.

doi:10.1371/journal.pgen.1001344.t001

uptaken by the BHK-21 cells, following application of the viruses to the cells (Figure 3B), and then the intracellular viral RNA levels increased rapidly and reached a maximum at 15 minutes post-infection (pi). The viral RNA levels remained approximately constant up to minute 60 pi, and then they increased exponentially. The uptake process was parallel for the two viruses. A similar result was observed upon measurement of the intracellular level of the two types of RNA during the exponential growth phase (Figure 3C). The slope of the exponential increase of intracellular RNA was parallel: the genomic intracellular RNA of C-S8p260 and C-S8p260p3d increased at a rate $r_{C\text{-}S8p260} = 0.050 \pm 0.004$ RNA molecules/cell·min and $r_{C\text{-}S8p260p3d} = 0.064 \pm 0.008$ molecules/cell·min , respectively ($F_{1,26} = 2.38$, $p = 0.13$, Figure 3C). The same culture samples were used to measure the release of viral RNA into the extracellular culture medium (Figure 3D). The results show that beginning at minute 135 pi, the concentration of extracellular viral RNA increased very rapidly at a similar rate of $r_{C\text{-}S8p260} = 0.076 \pm 0.008$ RNA molecules/cell·min and $r_{C\text{-}S8p260p3d} = 0.096 \pm 0.010$ molecules/cell·min ($F_{1,26} = 2.59$, $p = 0.12$). RNA samples were treated with RNase A (under the assumption that encapsidated RNA is RNase-resistant and non-encapsidated RNA is RNase-sensitive [7]), prior to the specific quantification of the two types of RNA. The treatment did not alter the measurements significantly (see Materials and Methods). Thus, the segmented and unsegmented forms of FMDV followed parallel kinetics of RNA synthesis, not only at the early steps of infection, but also during genome replication and release of RNA from the cell.

Kinetics of viral protein synthesis

The synthesis of viral proteins was analyzed at different times post-electroporation of BHK-21 cells with either RNA transcribed from plasmid pMT260p3d (that gives rise to C-S8p260p3d) or with an equimolar mixture of RNA obtained from plasmids pMT260Δ417ns and pMT260Δ999ns (that give rise to C-S8p260), constructed as described in Text S1 (Figure 3E, 3F and Figure S2). Electroporated and mock-electroporated cells were metabolically labeled with [^{35}S]Met-Cys, protein expression was monitored every 30 minutes, between 1.5 and 4.5 hours post-electroporation, and the proteins were resolved by SDS-PAGE and fluorography (Figure 3E). The analysis revealed a parallel expression kinetics of viral proteins, with few minor differences. In both cases, the maximum level of viral proteins was detected between 2 and 2.5 hours post-electroporation (Figure 3E, 3F). The expression of structural proteins VP1 and VP3 was lower in cells electroporated with RNA transcripts pMT260Δ417ns and pMT260Δ999ns than in cells electroporated with pMT260p3d. This may be a consequence of the deletion in pMT260Δ999ns that affects both the VP1 and VP3-coding regions. The kinetics of expression of non-structural proteins followed parallel curves during the time of the measurements, as determined by the label present in 3D and 3CD (Figure 3F). The results exclude that the selective advantage of population C-S8p260 can be due to faster kinetics in viral protein expression.

Specific infectivity and its relationship to fitness

To determine whether C-S8p260 and C-S8p260p3d displayed different specific infectivity (see Materials and Methods), viral genomic RNA molecules and infectivity (PFU/ml) were measured in both populations. Viral RNA production was 2.8±2.1 higher in C-S8p260p3d population relative to C-S8p260 population (repeated measures ANOVA: $F_{1,8} = 17.53$, $p<0.01$, Table 2). In agreement with this result, the production of viral particles was two-fold higher for C-S8p260p3d than for C-S8p260, as previously measured by quantitative electron microscopy [1]. Since both viruses, however, showed no differences in viral titer production (ANOVA: $F_{1,12} = 0.0018$, $p = 0.97$, Table 2), the specific infectivity of C-S8p260 is 2.6-fold higher than that of C-S8p260p3d. Of note, this difference coincides with the fitness differences between C-S8p260 and C-S8p260p3d (compare Table 1).

The ratio between the specific infectivities of C-S8p260 and C-S8p260p3d was additionally determined by using an alternative approach based on estimating the proportion of genomes that enter the cell for a given initial inoculum [8]. The ratio of C-S8p260 to C-S8p260p3d genomic RNA was measured in a mixture prepared with equal PFUs of C-S8p260 and C-S8p260p3d. Then, BHK-21 cells were infected with the mixture, and the ratio of segmented to ST RNA was determined 60 minutes after infection (before the onset of exponential replication). When complete cytopathic effect was reached, the ratio of the two types of RNA was measured again. The resulting cell lysate was used to infect new BHK-21 cells, and the process repeated to attain a total of three sequential cell entry events (Figure 4). The ratio of C-S8p260 to C-S8p260p3d RNA varied in a step-wise fashion, with 2-fold increases occurring only between each infection and the corresponding virus entry inside the cell. The magnitude of the step-wise increases confirmed the difference in specific infectivity between the two viruses (compare Figure 4 and Table 2). The ratio of the amount of the two types of RNA remained constant from each cell entry event up to the corresponding cell lysis, in agreement with the results of viral RNA kinetics (compare Figure 4 and Figure 3). The results strongly suggest that the viral population with the segmented genome is more infectious than the population with the ST genome. Upon elimination of the "Entry" points from the data in Figure 4, a graph coincident with that of a standard fitness determination is obtained (inset in Figure 4), which again indicates a two-fold higher fitness of C-S8p260 relative to C-S8p260p3d.

Comparison of virion stability

To investigate whether the increase of specific infectivity in the segmented-genome FMDV population could be attributed to an increase in the stability of the viral particles, the loss of infectivity of C-S8p260 and C-S8p260p3d at 37°C was quantitated. The results (Figure 5) show that the inactivation rate constant (see Materials and Methods) of C-S8p260 was $k = 0.0156 \pm 0.0005$ min^{-1} (correspond-

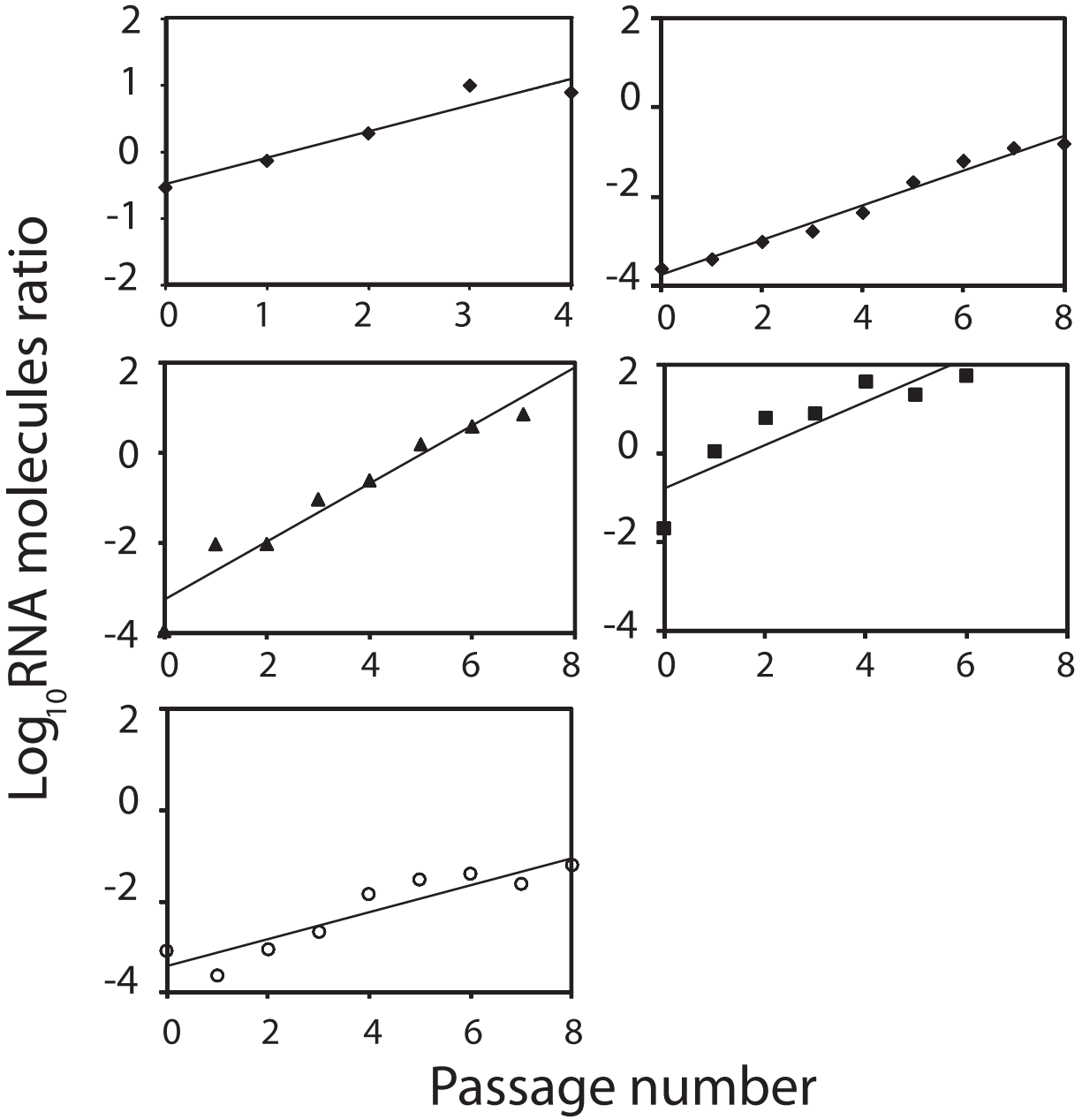

Figure 2. Growth-competition between FMDV mutants. At each time point (passage number), the ratio of RNA genomic molecules between the two competing viruses is represented. The data has been fitted to normalized exponential equations: (◆), left panel, C-S8p260/C-S8p260p3d ratio 1:1, $y = 1.1 \cdot e^{0.92\times}$, $R^2 = 0{,}92$; *right panel* C-S8p260/C-S8p260p3d ratio 1:1000, $y = 0{,}73 \cdot e^{0.90\times}$, $R^2 = 0{,}98$; (▲), C-S8p260/C$^9_{22}$L150: $y = 16.5 \cdot e^{1.251\times}$, $R^2 = 0{,}97$; (■), C-S8p260p3d/C$^9_{22}$L150: $y = 1{,}74 \cdot e^{0.701\times}$, $R^2 = 0{,}84$; (○), C-S8p260/C-S8p460p5d: $y = 2.16 \cdot e^{0.78\times}$, $R^2 = 0{,}87$. The results of fitness determinations are given in Table 1.
doi:10.1371/journal.pgen.1001344.g002

ing to a half-life of 44 min), while the inactivation rate constant of C-S8p260p3d was $k = 0.0190 \pm 0.0007$ min^{-1} (corresponding to a half-life of 33 min), a statistically significant difference (ANOVA, $F_{1.25} = 14.47$, $p < 0.001$). It must be noticed that both rates represent an extremely fast kinetics of infectivity decay, a well known feature of FMDV [9].

To establish a link between the stability of viral particles and the observed relationship of the fitness and infectivity differences between C-S8p260 and C-S8p260p3d, the infectivity of both populations was monitored again using the step-wise RNA level technique (described in Figure 4). Between the first and the second round of infection (that is, after the lysis event), the viral population was incubated for one additional hour at 37°C. The results indicate that the incubation at 37°C accentuated the increased infectivity of C-S8p260 relative to C-S8p260p3d (Figure 5C).

Thus, measurements of specific infectivity, virion stability, and the analysis of different steps involved in the virus life cycle suggest that increased stability of the particles harboring RNA with internal deletions is the phenotypic trait that conferred a selective advantage of the segmented virus over its ST counterpart.

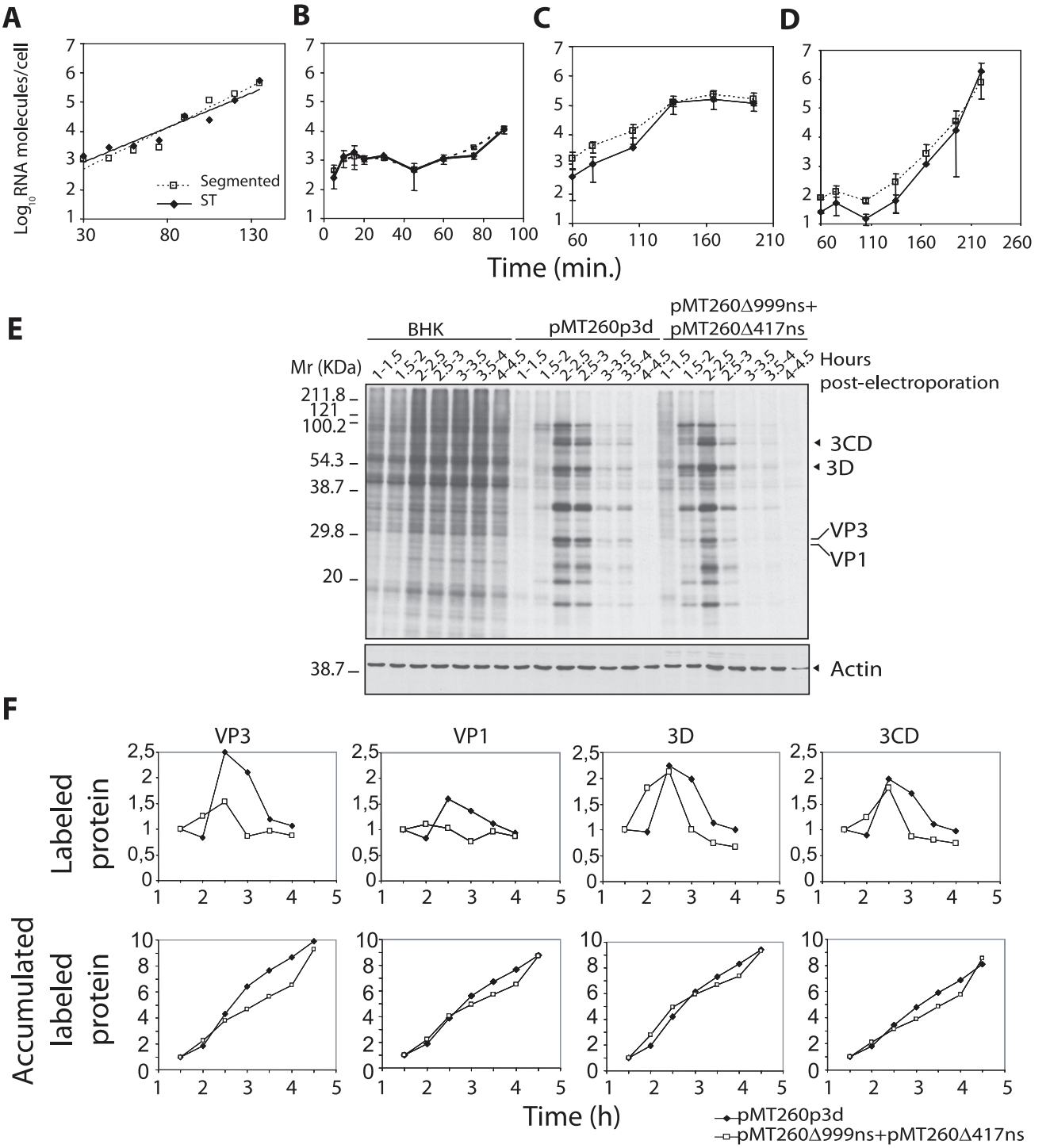

Figure 3. Replication kinetics of C-S8p260 (segmented) and C-S8p260p3d (ST) FMDV in BHK-21 cells. Cells were infected at a MOI of 20 PFU/cell. A to D) At different times after infection, the intracellular or extracellular concentration of genomic viral RNA (normalized to the number of cells) was determined. A) Intracellular concentration of viral RNA in two independent infections carried out in parallel; each value represents the average of two determinations. The data have been fitted to an exponential curve: C-S8p260: $4.8 \cdot 10^2 \cdot e^{0.065\times}$, $R^2 = 0.94$; C-S8p260p3d :$8.9 \cdot 10^2 \cdot 6e^{0.054\times}$; $R^2 = 0.92$. In B to D, BHK-21 cells were coinfected with the two viruses (C-S8p260 and C-S8p260p3d), at a MOI of 20 PFU/cell, and viral RNA was quantified as follows (symbols are as in A): B) Intracellular concentration of viral RNA in the course of virus entry into the cell. C) Intracellular viral RNA concentration during the exponential replication phase. D) Extracellular concentration of RNA measured in the cell culture supernatant obtained in the infection represented in C). In B–D the determinations were carried out from triplicate experiments (average values and standard deviation are shown). E) Electrophoretic analysis of ^{35}S-labeled proteins extracted from BHK-21 cells electroporated with FMDV RNAs. BHK-21 cells were either mock-electroporated (BHK lanes) or electroporated with transcripts from either pMT260p3d or a mixture of viral transcripts from pMT260Δ417ns and pMT260Δ999ns (which give rise to C-S8p260p3d and C-S8p260, respectively; see Figure S2). Parallel cultures were pulse-labeled with [^{35}S]Met/Cys for 30 min., at different times after 1 h post-electroporation, as indicated above each lane, and analyzed by PAGE, as described in Materials and Methods. The amount of cellular proteins was monitored by the relative amount of actin, visualized by Western-blot using a specific monoclonal antibody

(actin panels). F) The amount of viral proteins VP3, VP1, 3D and 3CD (in arbitrary units) at each time point was determined by densitometric scanning of the corresponding protein bands, and normalized to the concentration of actin (top panels). Values were added sequentially at each time point to obtain the accumulated level of viral protein (bottom panels).
doi:10.1371/journal.pgen.1001344.g003

Computational model

The empirical observations described can be synthesized in a simple computational model summarized in Figure 6. The standard type is termed population S, and the two complementing defective viruses are generically termed populations A (C-S8p260Δ417) and B (C-S8p260Δ999). Experiments on the kinetics of RNA and protein synthesis indicate that, in the replicative period inside the cell, particles of either type (S, A, or B) replicate at the same rate, conditional on at least one of their complementing counterparts being present for classes A and B. This condition is implemented as follows. Suppose that, initially, a cell holds n_S, n_A and n_B particles of types S, A, and B, respectively. After replication, the viral population is formed by $r\times M_A$ particles of type A, $r\times M_B$ particles of type B, and $r\times n_S$ particles of type S, where M_A is the smallest quantity of n_S+n_B and n_A, and M_B is the smallest quantity of n_S+n_A and n_B. On the other hand, experiments on specific infectivity and virion stability show that the segmented population is more infectious (due to its higher stability) than the standard counterpart. This is implemented as a decay factor $d_S<1$ that reduces the total number of S infective particles between replicative periods. In the particular case of the current experiments, a value of 0.47 can be estimated for the decay factor d_S (see Text S1). Those two steps (replication at the same rate and differential infection) quantify the process described in Figure 4. Finally, the average number of particles that infect cells is a constant m that stands for the MOI in the experimental system. In the experiments where the defective complementary form displaces S, $m=20$ has been used. The two key parameters are m and d_S, which represent antagonistic selection pressures. At low m, S populations are at an advantage because complementation is rare, while high m benefits segmented forms. However, the latter would be unable to displace the S population if both types were equally infectious. The increase in viral infectivity is truly beneficial for a value of m high enough that replication is not strongly limited by complementation. This is the behavior summarized in Figure 6, where the two different outcomes of the competition as a function of m and d_S are shown. Above a critical line of m values, there is co-dominance of standard and defective populations, while below that line the S population disappears.

The model correctly predicts that the standard form will be displaced by the complementary, defective population in the experimental situation (see Figure 6B), where the pair $(d_S, m)=(0.47, 20)$. It is important to emphasize that this result is independent of the fractions of S, A, and B present at the outset of the experiment or in the computational initial condition. Moreover, the inverse of the decay corresponds to the stepwise increase in the frequency of each virus, as displayed in Figure 4: $d_s^{-1}=1/0.47=2.1$. This value is in good agreement with empirical findings (see model prediction in Figure 4).

Discussion

Genome segmentation is a major evolutionary transition from independent towards complementing transmission of genetic information. Two main proposals for the evolutionary advantage of genome segmentation have been made on the basis of theoretical studies. One is that genome segmentation is a form of sex that counteracts the effect of deleterious mutations [5,10]. Another, not mutually exclusive but mechanistic proposal, is that genome segmentation may ensue from the selection of shorter RNA molecules whose replication is completed in a shorter time than replication of the corresponding full length genome [3,6]. Evidence supporting selection for deleted RNA was obtained in experiments involving *in vitro* replication of QβRNA, without the requirement to express viral proteins or to produce infectious particles [11,12]. In the case of FMDV there is no evidence of an advantage of the segmented over ST genome at the stage of RNA genome replication, protein expression or production of infectious virus, in agreement with previous descriptions for positive strand defective viruses [13,14]. The lack of replicative advantage of C-S8p260 is also reflected in the fact that the segmented virus had a constant two-fold additional fitness advantage, over the ST virus, independently of the genetic background of the competitor virus. Thus, all evidences point towards a non-replicative trait, virion stability, behind the selective advantage of the genome version with internal deletions. The slower inactivation rate of the segmented virus correlates with the difference of specific infectivity between C-S8p260 and C-S8p260p3d, and such a difference is, in

Table 2. Specific infectivity of FMDV populations C-S8p260 and C-S8p260p3d.

	Viral genomic RNA (molecules/ml supernatant)	Viral particles/μl supernatant[b]	Viral titer (PFU/ml)[c]	Specific infectivity[d]
C-S8p260p3d	$(9.5\pm0.8)\times10^{11}$[a]	$(1.5\pm0.6)\times10^{9}$	$(2.2\pm1.0)\times10^{8}$	2.4×10^{-4}
C-S8p260	$(3.6\pm1.7)\times10^{11}$[a]	$(5.5\pm0.8)\times10^{8}$	$(2.2\pm1.4)\times10^{8}$	6.3×10^{-4}
Ratio C-S8p260/C-S8p260p3d[e]	2.6 ± 0.47 (2.8 ± 2.1)[f]	2.73 ± 0.42	1 ± 0.4	0.38 (2.6)[g]

[a]Total viral RNA was measured in the supernatant of infected BHK-21 cells, when complete cytopathic effect was reached. Each value represents the mean and standard deviation of three independent determinations.
[b]These values were determined by quantitative electronic microscopy of purified viral stocks. Each value represents the mean and standard deviation of ten independent determinations.
[a,b]These values were reported in [1].
[c]Mean and standard deviation of 5 independent determinations.
[d]Ratio between viral genomic RNA molecules and viral titer.
[e]Ratio between values in the two first rows.
[f]In brackets, the average of seven additional determinations of the ratio between C-S8p260 RNA and C-S8p260p3d RNA is given.
[g]The inverse of 0.38 is given in brackets.
doi:10.1371/journal.pgen.1001344.t002

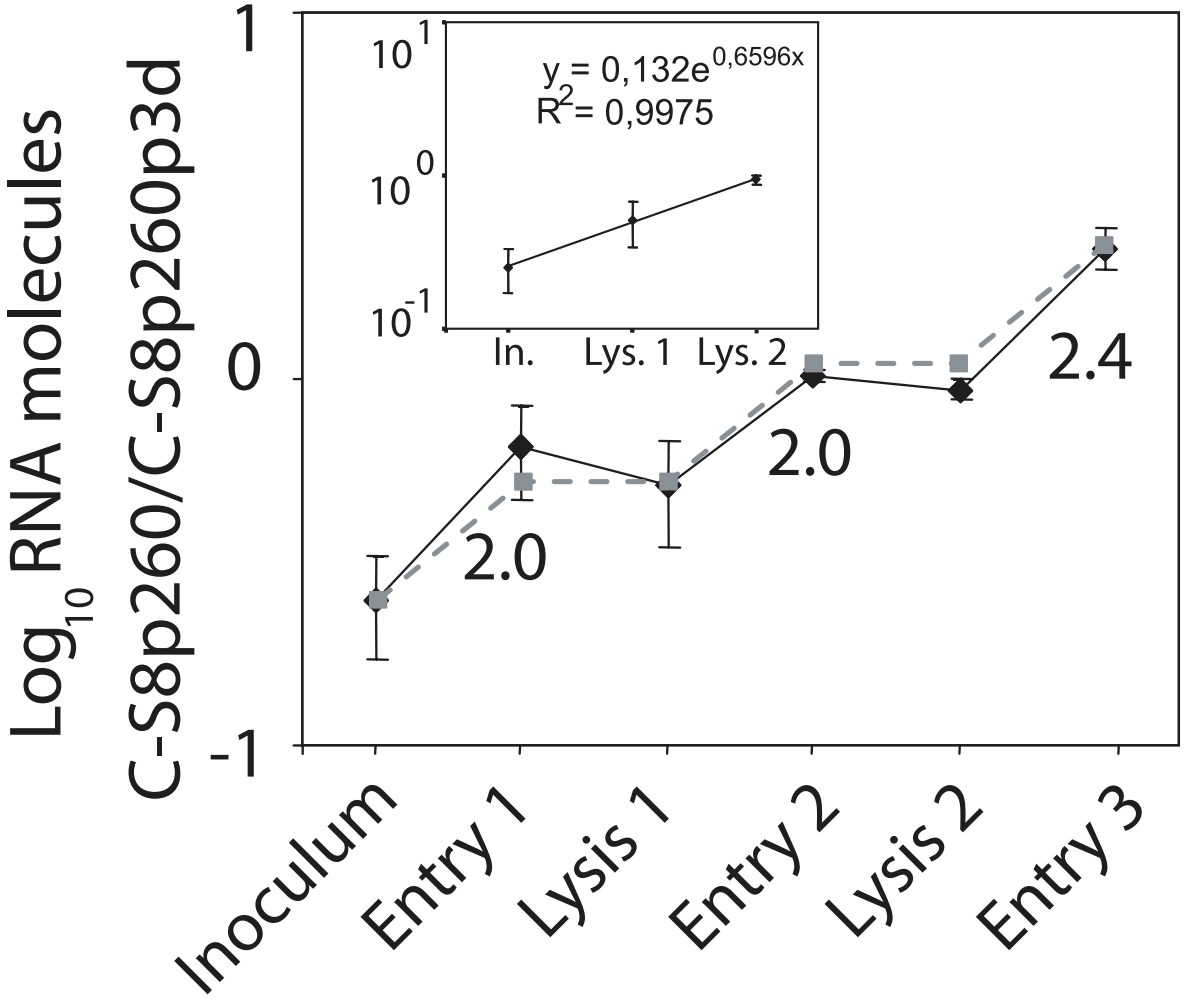

Figure 4. Dissection of the competition between C-S8p260 and C-S8p260p3d throughout sequential infectious cycles. BHK-21 cells were infected at a final MOI 20 PFU/cell with equal PFU of C-S8p260 and C-S8p260p3d. Each point of the black line represents the average and standard deviation of the ratio of genomic C-S8p260 and C-S8p260p3d RNA molecules, in five independent infections (except for the initial inoculum which was measured in three infections). In the abscissa, "Inoculum" is the ratio of the two RNAs in the viral stock used in the experiment. "Entry 1" is the RNA ratio at 60 minutes post-inoculation. "Lysis1" is the RNA ratio after complete cytopathic effect. The virus obtained from "Lysis 1" was used as the inoculum to perform the next infection which produced "Entry 2" and "Lysis 2". The infection to produce "Entry 3" was carried out with the virus obtained from "Lysis 2". The numbers adjacent to the lines indicate the increase in frequency of the genotype C-S8p260 at the corresponding step. The grey line was constructed by estimating the differential decay (d_s^{-1}) of the two viruses (see Text S1) during the time frame of one infection; the line assumes the same initial (inoculum) value and the same replication rate between "Entry" and "Lysis" points determined experimentally. The inset graph represents the exponential fit of the ratios obtained for "Inoculum" (In.), "Lysis 1" (Lys.1), and "Lysis 2" (Lys.2) from the black line. The relative fitness value calculated from this plot is 1.9. Procedures are detailed in Materials and Methods.
doi:10.1371/journal.pgen.1001344.g004

turn, at the origin of the fitness difference. Due to the exponential nature of the infectivity decay [15], even a modest increase in virion stability can account for the enrichment of the population in the more stable forms [13]. The implementation of the model with the actual values of the MOI and decay rates (see Text S1), estimated for the segmented and ST viruses, predicted a decay value (d_s) in the parameter space where the ST virus is driven to extinction. The inverse of this decay value ($d_s^{-1} = 2.1$) represents the relative increase per infection of the ST virus. This value confirms that the increased stability of the segmented virus can account for the differences in fitness, specific infectivity, and the step-wise dynamics observed (2.5, 2.6, and 1.9, respectively). The model also explores the limits imposed by the MOI on the complementing system, and predicts the minimal MOI required for the segmented forms to displace the ST virus.

The molecular basis for the higher thermal stability and fitness of the Infectious C-S8p260 population relative to the ST virus is unclear. However, some evidence indicates that thermal inactivation of FMDV may be due to a conformational change in the virion [9]. We suggest that the amount of RNA inside the virion may Influence the kinetic barrier of the inactivation process because of packaging considerations. The volume occupied per unit mass (V_m) [16] of full-length RNA inside the FMDV virion is about $V_m = 1.95$ Å^3/Da (see calculation of the RNA packaging density in the Text S1). This corresponds to a very high packing density, slightly higher than that of RNA in a molecular crystal (about 2.1 Å^3/Da), and substantially higher than the density of other icosahedral RNA viruses [17]. This measurement implies that genomes inside the capsid may be partially dehydrated. Packaging 5%–12% shorter RNAs (in the C-S8p260 virions)

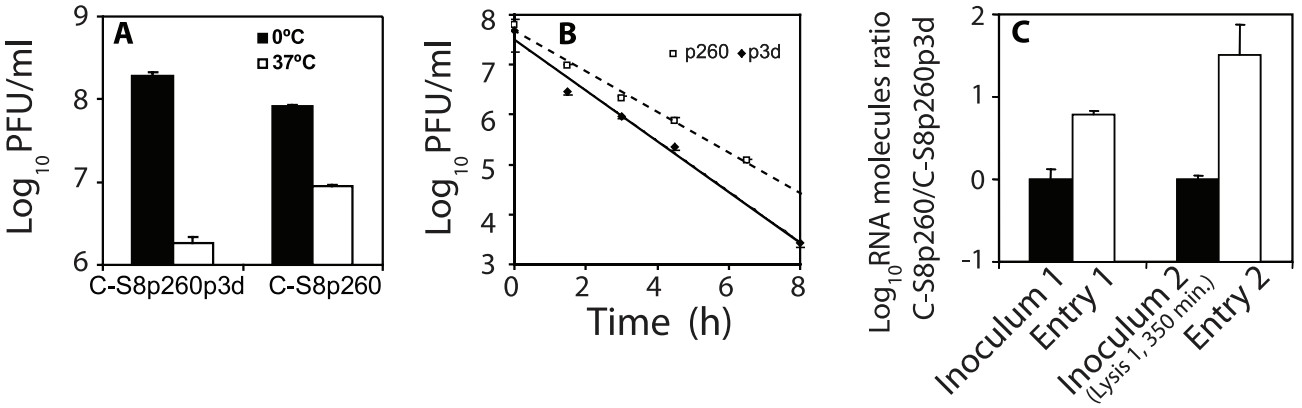

Figure 5. Decay of infectivity of FMDV particles. A) Equal volumes of C-S8p260p3d and C-S8p260 were incubated for two hours at 37°C or 0°C. The mean infectivity and standard error of triplicate experiments are plotted. B) Equal volumes of C-S8p260 and C-S8p260p3d were incubated at 37°C. Virus infectivity was determined, and plotted as a function of time. The decay of viral titer over time was fitted to a single exponential curve and the inactivation rate constant obtained. The equations that define the decay curves are: C-S8p260: $y = 4 \cdot 10^7 \cdot e^{-0.91 \cdot t}$, $R^2 = 0.995$; C-S8p260p3d: $y = 4 \cdot 10^7 \cdot e^{-1.19 \cdot t}$, $R^2 = 0.982$. C) BHK-21 cells were infected with equal number of PFUs of C-S8p260 and C-S8p260p3d, and the ratio of the two types of genomic RNA molecules was determined. "Inoculum 1" gives the RNA ratio in the viral stock used in the experiment. "Entry 1" indicates the RNA ratio at 60 minutes post-infection. When the cells reached complete cytopathic effect ("Lysis 1"), the supernatant was kept one additional hour at 37°C (350 minutes from the inoculation time). This supernatant corresponds to "Inoculum 2" and it was used to perform the next infection. "Entry 2" was measured after 60 minutes of infection with "Inoculum 2". Results are the average of 3 determinations, and standard deviations are given. Procedures are described in Materials and Methods.
doi:10.1371/journal.pgen.1001344.g005

would lead to Vm values of about 2.05 Å^3/Da–2.20 Å^3/Da, and thus may involve no dehydration. Based on these estimates, and ignoring other energetic effects on RNA packaging which are more difficult to predict, one could surmise that C-S8p260 virions would be at an energetically lower state than the ST virions harboring longer RNAs. The extra energy needed to trigger the putative conformational rearrangement that may lead to FMDV inactivation could be higher for the C-S8p260 virions than for the ST virions, rendering C-S8p260 virions more resistant to thermal inactivation, as experimentally observed. Accordingly, an increase in the length of an internal oligoadenylate tract in the viral RNA was shown to have a negative effect on FMDV fitness [18], and thermal stability [19]. Thus, variations of the RNA length could destabilize or stabilize the infectious virion conformation by reducing or increasing thermostability and fitness because of excessive RNA packing density, or by relaxing the RNA packaging

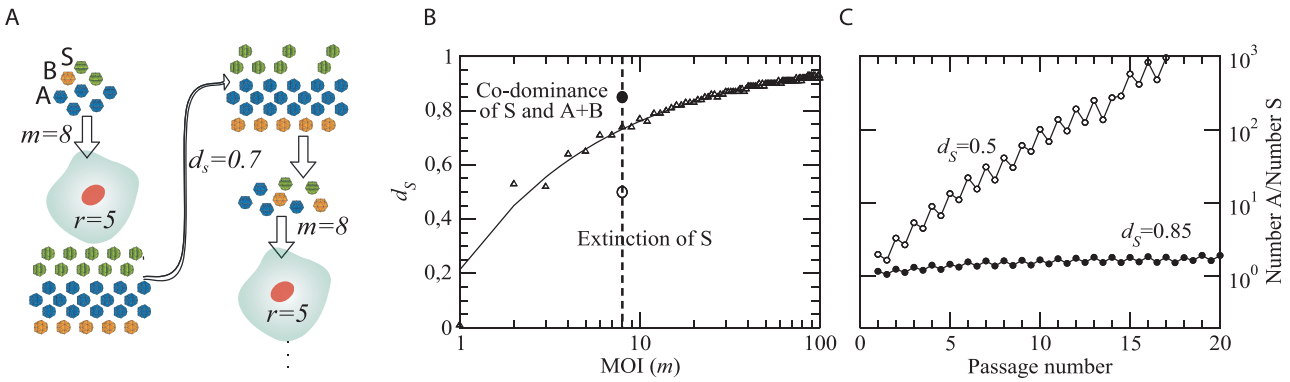

Figure 6. Computational model for the competition between ST and segmented forms. A cell is infected by *m* viral particles. All particles replicate inside the cell at the same rate *r*, conditional on having complementary partners in case they are defective. In the example shown, the replication of population A is limited by the presence of only three particles (one of type B and two standard) able to complement them. This replication process is repeated in *N* cells, and the total viral populations are summed up (not specified in this scheme). Before the process starts anew, the total standard population is reduced by a factor d_s, thus mimicking differential decay. For each cell at the next passage, a subset of *m* particles is randomly chosen among those remaining, and the process is repeated. B) The process described in A) has been iterated for 1000 passages. After that time, the composition of the population was analyzed. Triangles represent numerical results and indicate those parameter values where the composition changes from co-dominance (types A, B, and S present, above the triangles) to extinction of S (below); the line is a fit to the numerical data that yields the approximate relationship $d_s = 1 - m^{(-1/2)}$. C) Two representative examples of the kinetics of the ratio between the abundance of the population A and population S in the situations of extinction of the standard type (open circles in the upper curve correspond to the lower region in (A); $d_s = 0.5$) and of co-dominance (solid circles in the lower curve are representantive of the upper domain in (A); $d_s = 0.85$). Each curve yields the dynamics of the two points highlighted in (A) for $m = 8$, and the values of d_s are as indicated. In the co-dominance region, the fraction of A and S abundances reaches a constant value; in the region where the S form becomes extinct, the abundance of A relative to S grows exponentially fast in successive passages until S is eventually displaced.
doi:10.1371/journal.pgen.1001344.g006

constraints, respectively. Packaging constraints of genome length in icosahedral viruses have been previously described, including adenovirus vectors [20] or the strongly pressurized capsids of some double-stranded DNA viruses [21]. A study including multiple DNA and RNA bacteriophages concluded that genome packaging density was negatively correlated with virus stability [22]. Gene overlapping in viruses is thought to have evolved as a consequence of physical constraints of genome length in the capsid [23]. Accordingly, our results contribute a new model for the fitness advantage of RNA genome segmentation, a key evolutionary transition in RNA genetics. We propose that segmentation is a molecular solution that counteracts the trade-off between capsid stability and genome length in geometrically constrained viral particles. The relaxation of the genome packaging of segmented genomes maximizes the genetic content in the virion without the associated loss of particle stability.

Materials and Methods

Cells, viruses, and infections

The origin of baby hamster kidney 21 (BHK-21) cells and procedures for cell growth, infection of cell monolayers with FMDV in liquid medium, and for plaque assays in semisolid agar medium have been previously described [18,24]. FMDV C-S8c1 is a plaque-purified virus of natural isolate C1 Santa-Pau Spain 70 [24]. FMDV C-S8p260 and C-S8p460 are the viral populations obtained after 260 and 460 serial cytolytic passages, respectively, of C-S8c1 at high MOI in BHK-21 cells (2×10^6 BHK-21 cells infected with the virus contained in 200 µl of the supernatant from the previous infection, that include about $2\cdot10^6$ to $4\cdot10^7$ PFU) (Figure S1) [1,2]. FMDV C-S8p260p3d and C-S8p460p5d are the viral populations obtained after three serial cytolytic passages of C-S8p260 and five serial cytolytic passages of C-S8p460, respectively, at low MOI in BHK-21 cells (2×10^6 BHK-21 cells infected with 200 µl of a 10^{-3} dilution of the supernatant from the previous infection; MOI of about 10^{-3} PFU/cell) [1,2]. FMDV $C^9{}_{22}$L150 was obtained after 150 population passages of clone $C^9{}_{22}$ (a subclone of C-S8c1 p2) in BHK-21 cells (MOI of 0.1–10 PFU/cell) [25]. The production of lytic plaques (used to determine the viral titer) in a population of complementing viruses follows a two-hit kinetics as described in [26] and in the Text S1.

RNA quantification, cDNA synthesis, PCR amplification, and nucleotide sequencing

Viral RNA was extracted from the viral samples using Trizol (Invitrogen). Intracellular RNA was extracted by direct addition of Trizol to the cell monolayer, after removing the cell culture medium. RNA was quantified by real-time RT-PCR with the Light Cycler instrument (Roche) using the Light Cycler RNA Master kit (Roche), as previously described [27]. Purified RNA from FMDV C-S8p260p3d or pMT260Δ999ns was used as standard. Reverse transcription was performed with AMV reverse transcriptase (Promega), and PCR amplification was carried out using Ampli-Taq polymerase (Perkin-Elmer), as specified by the manufacturers. The pairs of sense and antisense oligonucleotides, respectively, that amplify specific viruses are the following: C-S8p260p3d, 5′-CTACCCATGGACGCCAGACCCG-3′ (sense)/5′-GTGTTGGTTGTGTGTGCAG-3′ (antisense); C-S8p260, 5′-CACGAATTCACGGGCAAAGGCTACTGG-3′ (sense)/5′-GAGAAGAAGAAGGGCCCAGGGTTG-3′ (antisense).

RNase A treatment

When necessary, the supernatants of infected cells were treated for 1 hour with 1 µg/ml of pancreatic RNase A as previously described [7], to eliminate non-encapsidated RNAs. Six independent samples of the supernatant of BHK-21 cells coinfected by C-S8p260 and C-S8p260p3d were either untreated or treated with RNase, prior to the specific quantification of the two types of RNA by real-time RT-PCR, as described in [7]. The ratio of segmented to unsegmented genomic RNA was $1{,}23\pm1{,}11$ in RNase A-treated and $1{,}64\pm0{,}49$ in untreated samples. Thus, no significant differences (ANOVA, $F_{1.10}=0.68$, $p>0.43$) could be detected between the amounts of encapsidated and non-encapsidated genomic RNA released into the culture medium by the segmented and ST viruses.

Specific infectivity is defined as the ratio between the number of infectious viruses, measured in PFUs, and the total amount of viral RNA, determined by quantitative RT-PCR.

Kinetics of viral RNA synthesis

BHK-21 monolayers of $5\cdot10^5$ cells were infected in parallel with $1\cdot10^7$ PFU of C-S8p260, C-S8p260p3d or the mixture of both (a total of $2\cdot10^7$ PFU). At each specific time point, at least three plates were withdrawn for the determination of intracellular and extracellular FMDV RNA. The RNA values obtained were normalized to the number of cells. The increase of the amount of viral RNA over time was fitted to the equation: $x(t)=x_0\cdot e^{(r\cdot t)}$, where r is the growth rate constant measured in RNA molecules/passage. During coinfections, the concentration of C-S8p260 was measured by RT-PCR amplification using primers that specifically amplify the genome harboring deletion Δ999. Since this genome has been estimated in a proportion of 40% in the C-S8p260 population [1], viral RNA of C-S8p260 population has been calculated as 2.5 times the concentration of Δ999 RNA.

Protein analysis and fluorography

Viral protein synthesis was analysed by metabolic pulse-labelling with [^{35}S] Met-Cys, followed by SDS-PAGE electrophoresis and fluorography. Proteins were labelled by the addition of 60 µCi of [^{35}S] Met-Cys (Amersham) per ml in methionine-free DMEM. Fluorography, autoradiography and western blot procedures of the gels were carried out as previously described [28]. The amount of actin in the sample was determined using anti-β-actin MAb AC-15 (Sigma), and corresponded to a concentration of protein in the linear region of the relationship between the western blot signal and the protein concentration. FMDV-specific proteins were identified using MAbs [29], as previously described [30].

Virus growth-competition assays

Growth-competitions between two viruses in BHK-21 cells were carried out as previously described [25], with minor modifications. A cell monolayer is infected with a mixture of a problem and reference virus in a proportion of 1:1000 (unless otherwise stated) and at a MOI = 10–20. When the complete cytopathic effect is reached the supernatant (containing the virus) is collected and used for a new infection. The fitness of several clones used in the present study is considerably high. Moreover, fitness determination of a multipartite virus does not have a standardized protocol. Using the ratio 1:1000 allows performing 6 to 8 serial infections (the typical number being 3 to 4) before the exponential variation of the genotypes frequency reaches a saturation point. The exponential increase of the proportion of the problem genomes is fitted to an exponential curve. The slope of the curve gives the selection coefficient for one strain relative to the other [31]. This value is often used in virology as a measure of the relative fitness [32]. The proportion of the two genomes at different passages was determined by specific real-time RT-PCR. The equations for

each competition and fitness values are given in the legend of Figure 2 and in Table 1, respectively.

Measurements of infectivity decay

Equal volumes of viral samples of C-S8p260 and C-S8p260p3d were incubated at 37°C and aliquots were collected at different time points and rapidly chilled to 0°C. Viral titer decay as a function of time was determined and fitted to an exponential curve following the equation: *viral titer (at time t) = viral titer (at time t = 0)* · $e^{-k \cdot t}$, where $k(h^{-1})$ is the inactivation rate constant of the infectious FMDV virion [33]. The equations that define the inactivation rate and the average life of the segmented and ST viruses are given in the legend of Figure 5.

Statistical analysis

One Way ANOVA were calculated using the Statistica 6.0 software package (StatSoft 2001).

Supporting Information

Figure S1 FMDV genome and position of internal deletions identified upon passage of biological clone C-S8c1 in BHK-21 cells. A) Scheme of the FMDV genome (C-S8c1 or its infectious transcript pMT28), with non-coding regions depicted as lines and the encoded proteins as boxes. VPg (or 3B) is the protein covalently linked to the 5′-end of the RNA, poly C is the internal polycytidylate tract, and (A)n is the 3′-terminal poly A. The four main coding regions (L, P1, P2, P3) are indicated. B) Serial passages of FMDV clone C-S8c1 (filled square), and the types of genomes identified in different passages. The number following Δ indicates the size of the deletion in base pairs. The position of a deletion is shown as a black segment within the genome (compare with A). FMDV populations are depicted as open circles; large grey arrows indicate high MOI passages (2–20 PFU/ml); the number following p indicates passage number. Populations C-S8p260p3d and C-S8p460p5d were derived from C-S8p260 and C-S8p460 by three and five low MOI (0.02 PFU/cell) passages, respectively (thin arrow-heads). C-S8p260p3d and C-S8p460p5d included ST RNA as the only detectable genome.
Found at: doi:10.1371/journal.pgen.1001344.s001 (0.86 MB EPS)

Figure S2 Construction of plasmids pMT260 Δ 417ns, pMT Δ 999ns and pMT260p3dns. The plasmids pMT260 Δ 417ns and pMT Δ 999ns (see Text S1) were prepared from the corresponding plasmids pMT Δ 417 and pMT Δ 999, whose construction was previously described [1]. The infectious transcript pMT28, which encodes the sequence of C-S8c1, is depicted in grey, as represented in Figure S1. Genomic regions from C-S8p260p3d are depicted in color. Critical restriction sites are indicated by arrows. pMT260 Δ 417ns and pMT Δ 999ns were constructed to include the ns region (genomic residues 4201 to 7427) of C-S8p260p3d (last scheme). pMT260p3d was constructed by replacing the genomic region spanning residues 638 to 2046 from pMT260 Δ 417ns by the same region from pMT260 Δ 999ns.
Found at: doi:10.1371/journal.pgen.1001344.s002 (3.60 MB EPS)

Text S1 Supplementary Materials and Methods.
Found at: doi:10.1371/journal.pgen.1001344.s003 (0.10 MB DOC)

Acknowledgments

We thank David Baltimore for the critical reading of the manuscript. We also thank M. Dávila and A. I. de Ávila for technical assistance.

Author Contributions

Conceived and designed the experiments: SO CE SCM ED. Performed the experiments: SO CP MGM. Analyzed the data: SO JGA CE SCM CP MGM ED. Contributed reagents/materials/analysis tools: JGA AA. Wrote the paper: SO SCM MGM ED.

References

1. Garcia-Arriaza J, Manrubia SC, Toja M, Domingo E, Escarmis C (2004) Evolutionary transition toward defective RNAs that are infectious by complementation. J Virol 78: 11678–11685.
2. Garcia-Arriaza J, Ojosnegros S, Davila M, Domingo E, Escarmis C (2006) Dynamics of mutation and recombination in a replicating population of complementing, defective viral genomes. J Mol Biol 360: 558–572.
3. Nee S (1987) The evolution of multicompartmental genomes in viruses. J Mol Evol 25: 277–281.
4. Szathmary E (1992) Natural selection and dynamical coexistence of defective and complementing virus segments. J Theor Biol 157: 383–406.
5. Chao L (1988) Evolution of sex in RNA viruses. J Theor Biol 133: 99–112.
6. Holmes EC (2009) The Evolution and Emergence of RNA Viruses; Harvey PM, May RM, eds. Oxford: Oxford University Press.
7. Escarmis C, Carrillo EC, Ferrer M, Arriaza JF, Lopez N, et al. (1998) Rapid selection in modified BHK-21 cells of a foot-and-mouth disease virus variant showing alterations in cell tropism. J Virol 72: 10171–10179.
8. Barclay W, Li Q, Hutchinson G, Moon D, Richardson A, et al. (1998) Encapsidation studies of poliovirus subgenomic replicons. J Gen Virol 79(Pt 7): 1725–1734.
9. Mateo R, Luna E, Rincon V, Mateu MG (2008) Engineering viable foot-and-mouth disease viruses with increased thermostability as a step in the development of improved vaccines. J Virol 82: 12232–12240.
10. Szathmary E (1992) Viral sex, levels of selection, and the origin of life. J Theor Biol 159: 99–109.
11. Mills DR, Peterson RL, Spiegelman S (1967) An extracellular Darwinian experiment with a self-duplicating nucleic acid molecule. Proc Natl Acad Sci USA 58: 217–224.
12. Sabo DL, Domingo E, Bandle EF, Flavell RA, Weissmann C (1977) A guanosine to adenosine transition in the 3′ terminal extracistronic region of bacteriophage Qβ RNA leading to loss of infectivity. J Mol Biol 112: 235–252.
13. Cole CN, Baltimore D (1973) Defective interfering particles of poliovirus. IV. Mechanisms of enrichment. J Virol 12: 1414–1426.
14. Lundquist RE, Sullivan M, Maizel JV, Jr. (1979) Characterization of a new isolate of poliovirus defective interfering particles. Cell 18: 759–769.
15. Nowak MA, May RM (2000) Virus Dynamics. Mathematical Principles of Immunology and Virology. New York: Oxford University Press Inc.
16. Matthews BW (1968) Solvent content of protein crystals. J Mol Biol 33: 491–497.
17. Johnson JE, Rueckert RR (1997) Packaging and release of the viral genome. In: Chiu W, Burnett RM, Garcea RL, eds. Structural Biology of Viruses. New York: Oxford University Press. pp 269–287.
18. Escarmis C, Davila M, Charpentier N, Bracho A, Moya A, et al. (1996) Genetic lesions associated with Muller's ratchet in an RNA virus. J Mol Biol 264: 255–267.
19. Diez J, Davila M, Escarmis C, Mateu MG, Dominguez J, et al. (1990) Unique amino acid substitutions in the capsid proteins of foot-and-mouth disease virus from a persistent infection in cell culture. J Virol 64: 5519–5528.
20. Bett AJ, Prevec L, Graham FL (1993) Packaging capacity and stability of human adenovirus type 5 vectors. J Virol 67: 5911–5921.
21. Gelbart WM, Knobler CM (2009) Virology. Pressurized viruses. Science 323: 1682–1683.
22. De Paepe M, Taddei F (2006) Viruses' life history: towards a mechanistic basis of a trade-off between survival and reproduction among phages. PLoS Biol 4: e193. doi:10.1371/journal.pbio.0040193.
23. Chirico N, Vianelli A, Belshaw R Why genes overlap in viruses. Proc Biol Sci 277: 3809–3817.
24. Sobrino F, Davila M, Ortin J, Domingo E (1983) Multiple genetic variants arise in the course of replication of foot-and-mouth disease virus in cell culture. Virology 128: 310–318.
25. Escarmis C, Davila M, Domingo E (1999) Multiple molecular pathways for fitness recovery of an RNA virus debilitated by operation of Muller's ratchet. J Mol Biol 285: 495–505.
26. Manrubia SC, Garcia-Arriaza J, Escarmís C, Domingo E (2006) Long-range transport and universality classes in in vitro viral infection spread. Europhysics Letters 74: 547–553.
27. Perales C, Agudo R, Tejero H, Manrubia SC, Domingo E (2009) Potential benefits of sequential inhibitor-mutagen treatments of RNA virus infections. PLoS Pathog 5: e1000658. doi:10.1371/journal.ppat.1000658.
28. Perales C, Mateo R, Mateu MG, Domingo E (2007) Insights into RNA virus mutant spectrum and lethal mutagenesis events: replicative interference and complementation by multiple point mutants. J Mol Biol 369: 985–1000.

29. Mateu MG, Martinez MA, Capucci L, Andreu D, Giralt E, et al. (1990) A single amino acid substitution affects multiple overlapping epitopes in the major antigenic site of foot-and-mouth disease virus of serotype C. J Gen Virol 71(Pt 3): 629–637.
30. Escarmis C, Perales C, Domingo E (2009) Biological effect of Muller's Ratchet: distant capsid site can affect picornavirus protein processing. J Virol 83: 6748–6756.
31. Maree AF, Keulen W, Boucher CA, De Boer RJ (2000) Estimating relative fitness in viral competition experiments. J Virol 74: 11067–11072.
32. Holland JJ, de la Torre JC, Clarke DK, Duarte E (1991) Quantitation of relative fitness and great adaptability of clonal populations of RNA viruses. J Virol 65: 2960–2967.
33. Mateo R, Luna E, Mateu MG (2007) Thermostable variants are not generally represented in foot-and-mouth disease virus quasispecies. J Gen Virol 88: 859–864.